Loading Slim Hot Water Tanks With and Without Swirl Generation - First Results

Felix Oestreich[1], Thorsten Urbaneck[1]

[1] Chemnitz University of Technology, Professorship Applied Thermodynamics, Chemnitz (Germany)

Abstract

Hot water storage tanks (pressure vessels) enable the storing of pressurized water in the temperature range 95…200 °C. These storage tanks are often used in solar heat supply systems, in combined heat and power plants, in district heating networks and in industrial heat supply networks. During loading, flow effects occur in slim storage tanks, which are detrimental to the development of thermal stratification. This work compares the thermal stratification development for loading with conventional radial diffusers with a new diffuser design that generates swirl flow. Numerical flow simulation (CFD) studies show the behaviour in the diffuser and in the storage. The effects on thermal stratification are analysed and evaluated with known key figures.

Keywords: thermal energy storage, tank, pressure vessel, hot water, heat supply, stratification, charging device, diffuser, optimization, swirl, simulation

1. Introduction

To achieve the goals of the Paris climate agreement, the reduction of greenhouse gas emissions in the area of energy supply is essential (BMUV, 2022). The supply of space heating and tap water as well as the provision of process heat (56 % of final energy consumption in Germany, as of 2020) cause a large part of these emissions (AG Energiebilanzen, 2022). Therefore, the development of renewable energy supply is necessary for a climate-neutral or emission-free heat supply. Medium-temperature solar thermal energy can make a significant contribution in the area of district heating supply. This is confirmed, for example, by the studies of *Stahlhut* et al. (Stahlhut, 2022a, 2022b). The provision of heat by collector fields is predominantly time-delayed to the heat demand. Thermal energy storage systems can store surplus heat and supply it to the heating network or consumers with a time delay. In this way, the storage units enable a temporal decoupling. In district heating supply, hot water storage tanks fulfill this function.

Available storage tank designs are shown in Fig. 1 (Urbaneck, 2020). For the temperature range 95...140 °C, flat-bottom tanks are suitable as two-zone storage tanks (a4) as well as slim pressure vessels (b1) and compact pressure vessels (b2). This work deals with slim pressure vessels (b1). Fig. 2 shows such an installation with slim tanks. The operating pressure of 10 to 20 bar enables the storage of liquid water from 95 to approx. 200 °C. This means that these storage tanks are also suitable for industrial heat supply. Fig. 3 shows the specific storage investment costs for all storage types from Fig. 1. Consequently, storage design (b1) is particularly advantageous for high temperature differences (> 75 K) and medium storage capacities up to 400 MWh compared with other storage designs (Urbaneck, 2020).

Due to production in the factory, typical storage volumes are between 180 and 200 m³ per storage tank (Fig. 2). The schematic structure of a series connection of storage tanks (b1) is shown in Fig. 4. Larger storage volumes can be realized via series and parallel connection (Fig. 2). The storage are operated according to the displacement principle. The pressure is maintained outside the storage so that the storage are completely filled with water.

The operation of such storage facilities is complex and depends on many influencing factors. One essential aspect is the thermal stratification. The stratification characterizes the vertical temperature distribution and provides information about mixing processes in the storage tank. A high quality of thermal stratification indicates low internal storage losses. Internal storage losses are the temperature reduction of the storage water by mixing or heat conduction as well as further heat transfer processes in the storage. These losses can be described by the increase of entropy or the decrease of exergy. A significant influence on the stratification quality has the operating parameters (e.g. density difference, volume flow rate) during the loading process and the design (geometry, shape) of the loading system. The aim of this work is to improve the thermal stratification during the loading process of slim hot water storage tanks. The investigations are carried out with numerical flow simulation (CFD). The flow processes or heat transfer in the loading system and in the storage room were modeled. External losses (e.g. heat transfer processes in the storage tank wall) are not subject of this investigation.

doi:10.18086/eurosun.2022.13.14 Available at http://proceedings.ises.org

In order to achieve an improvement of the thermal stratification, different diffuser designs are investigated. A conventional radial diffuser is used for loading (Fig. 5 a)). This diffuser allows radial velocity decay and theoretically uniform inflow (equal distribution of direction and velocity at the diffuser outlet) of the loading fluid into the storage. Fig. 5 b) shows this behaviour in a very simplified way. In principle, this behavior is favorable for building up the thermal stratification.

Studies by (Brähmer, 2012) and (Lohse, 2012) show that, due to the relatively small storage radius, undesirable flow effects occur (e.g. formation of a wall jet and a large-scale mixing zone in the upper storage area), which lead to a poor starting position with regard to the stratification structure. To overcome this flow problem, (Platzer, 2017) proposes swirl loading. For swirl generation, guide elements are installed in the diffuser (Fig. 5 c)). These internal elements are characterized by the entrance α, the exit angle or swirl angle β and the number of internal elements z (Fig. 5 d)). The rotation is intended to reduce the momentum of the jet in the upper storage region. This fundamentally changes the flow behaviour (Fig. 5 e)), novel loading with swirl generation). First empirical investigations showed the advantageousness (Winkler, 2017). Subsequent experimental work did not provide clear results (Kroll 2020a, 2020b). Therefore, it must be fundamentally clarified whether loading with swirl has a positive influence on the quality of thermal stratification. For further optimization of the loading, a better understanding of the flow processes during loading with swirl generation is urgently needed as a next step.

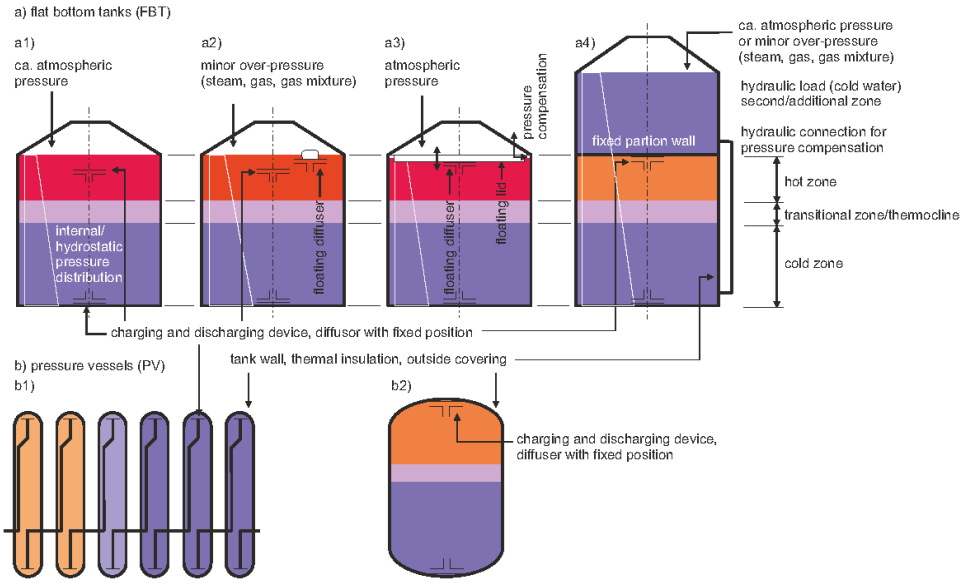

Fig. 1: Systematization of known tank storage constructions (Urbaneck 2020)

Fig. 2: Slim hot water storage tanks, four times nine storage tanks in series, Chemnitz (Germany) district heating supply, operator eins/inetz

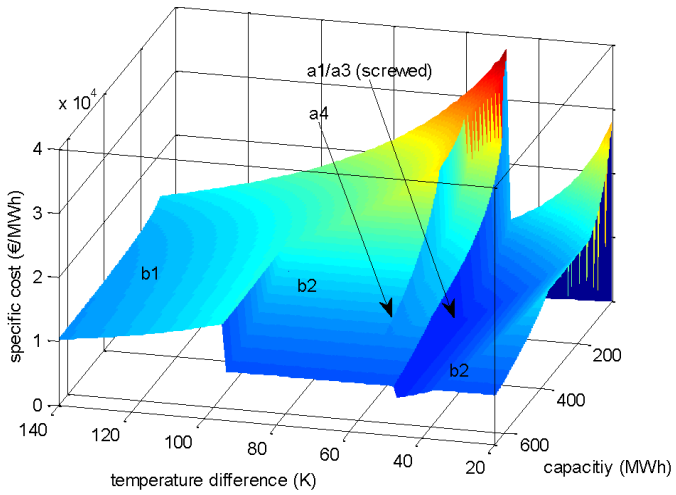

Fig. 3: Specific costs depending on storage capacity and temperature difference, cost calculation 2018 (Urbaneck 2020)

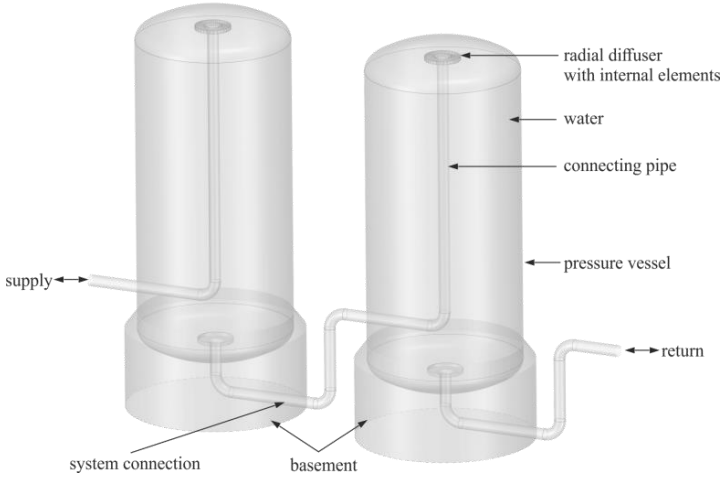

Fig. 4: Schematic structure of the storage type b1 (representation with low storage height) in a series connection, without thermal insulation, covering and auxiliary equipment

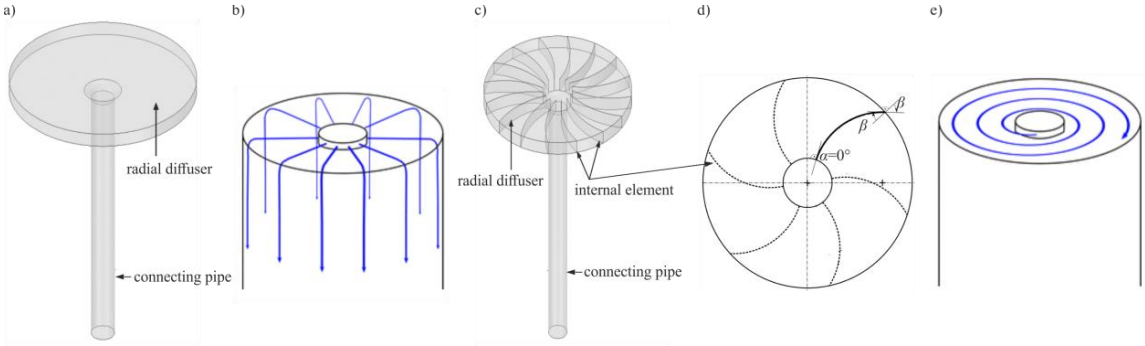

Fig. 5: a) radial diffuser, b) simplified representation of radial charging c) radial diffuser with internal elements, d) design sketch with selected parameters, e) simplified representation of charging with swirl generation (Winkler 2017)

2. Simulation

The Ansys CFD software is used to simulate the flow and heat transfer (Ansys, 2019). The simulation models for the diffuser and the storage are shown in Fig. 6. This division of the region and the use of sections reduces the computational effort. This means, there is no complete modelling of the storage space.

The geometric quantities are summarized in Tab. 1. These investigations refer to a simplified storage geometry

(cylinder) without dished bottom. The storage model considers the upper storage area with 30 % of the real storage height h_{St}. This is sufficient for the simulation of the loading behaviour (Urbaneck, 2019).

This paper presents two modeling variants. In variant *a*, only the storage model (Fig. 6 b)) is used. At the inlet the velocity components (Fig. 6 b)) are defined for the conventional diffuser (Fig. 5 a) and the diffuser with swirl generation (Fig. 5c)). Then there is an ideal uniform distribution of the velocity field. This means, the flow in the connecting pipe and diffuser is not considered.

In variant *b*, the diffuser model (Fig. 6 a)) should generate realistic inlet boundary conditions for the storage model (Fig. 6 b)). Therefore, the simulation is performed in two steps. First, the diffuser model is simulated. The results include the temperature and velocity field at the diffuser outlet. This is imposed as inlet boundary condition (inlet) on the storage model. In this investigation, the diffuser with swirl has a number of internal elements of 128 and 32, respectively, and a swirl angle of 50° and 10°, respectively. Then the section angle is 2.8° or 11.25°. The variants are then called *RD IE 128 50°* or *RD IE 32 10°*. The preliminary investigations in (Winkler, 2017) showed that these variants have advantages over the conventional diffuser (designation *RD*).

The simulations represent an ideal loading (e.g. constant temperature, constant volume flow). The storage geometry and the boundary conditions for the loading remain constant for all variants. The simulated loading time is 250 s. Then the thermal stratification is formed. The time step size is 0.1 s. For turbulence modeling, the $k-\omega$ −SST model with consideration of buoyancy is applied. Work by (Findeisen, 2016) shows the suitability of this turbulence model. The determination of the temperature- and pressure-dependent material values is done with the industrial formulation IAPWS-IF97 (Wagner and Kretzschmar, 2008). At time t = 0 s, the quiescent storage fluid (water) has a constant temperature. The evaluation refer to the end of the simulation at time t = 250 s. The horizontal evaluation planes (Fig. 6 a), yellow plane) are located at h_D= (0.025, 0.050, 0.075) m. The vertical evaluation line (Fig. 6 a), black plane) runs in the middle of the section.

Tab. 1: Geometrical sizes of the storage and the radial diffuser

quantity	value	quantity	value
h_{St} [m]	10.00	r_{CP} [m]	0.16
r_{St} [m]	2.00	h_{CP} [m]	1.50
r_D [m]	0.50	z [-]	32 / 128
h_D [m]	0.10	β [°]	10 / 50

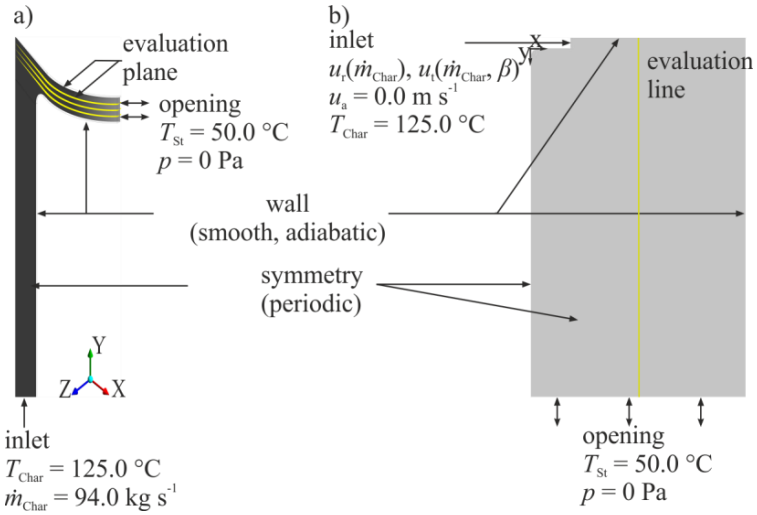

Fig. 6: Schematic representation of a) the diffuser model (curved section) and b) the storage model (normal circular section) with boundary condition for the numerical flow simulation (CFD)

3. Evaluation of the Thermocline

For the evaluation of the thermal stratification, three zones are defined in the first step (Fig. 7): the hot zone, the thermocline and the cold zone. The spatial distribution of these zones cannot be precisely determined due to the sliding vertical temperature distribution. Therefore, in the literature one can find different rules for the determination. In this work the following evaluation criteria are used: the average height of the thermocline $h_{\mathrm{tc,m}}$, the maximum temperature gradient $(\mathrm{grad}T_{St})_{\mathrm{max}}$, the average temperature in the warm zone T_{hZ}. The parallel use of different evaluation criteria allows a better analysis, because each criterion has advantages and disadvantages.

The 90/10% criterion is used to determine the average height of the thermocline $h_{\mathrm{tc,m}}$ (Fig. 7). The highest temperature $T_{\mathrm{St,max}}$ = 125 °C corresponds to the temperature of the loading fluid. The limit temperature for the hot zone is set at $T_{\mathrm{St,90\%}}$ = 117.5 °C (eq. 1). A set temperature for the supply of a network $T_{\mathrm{Su,S}}$ is often defined, e.g. for the flow of a heat distribution network. This target flow temperature defines the minimum permissible temperature for network operation. This means that the storage tank can only be discharged as long as this criterion is met. Thus, the set flow temperature limits the discharge. In this work, the following condition shall apply: $T_{\mathrm{St,90\%}} = T_{\mathrm{Su,S}}$. Beneath $T_{\mathrm{St,10\%}}$= 57.5 °C (eq. 2) is the cold zone. The lowest temperature $T_{\mathrm{St,min}}$ = 50 °C corresponds to the temperature of the storage fluid at the beginning of loading. Between both zones lies the thermocline. A reduction of the thermocline proves the advantage of a loading technique or a certain variant, which corresponds to the general aim of this work.

In Fig. 7, the zones are described with a horizontal line, which corresponds to a constant horizontal temperature. During loading, the flow processes in reality and in the simulation cause wavy boundaries between the zones. Therefore, the surfaces with temperatures $T_{\mathrm{St,90\%}}$ and $T_{\mathrm{St,10\%}}$ are spatially determined with a relatively new evaluation method. In *Ansys CFD Post*, the so-called *isosurfaces* are applied. Then the height of the thermocline can be calculated in every point (Findeisen 2016).

$$T_{\mathrm{St,90\%}} = T_{\mathrm{St,min}} + 0{,}9 \cdot (T_{\mathrm{St,max}} - T_{\mathrm{St,min}}) \qquad \text{(eq. 1)}$$

$$T_{\mathrm{St,10\%}} = T_{\mathrm{St,min}} + 0{,}1 \cdot (T_{\mathrm{St,max}} - T_{\mathrm{St,min}}) \qquad \text{(eq. 2)}$$

The vertical temperature gradient $\mathrm{grad}T_{\mathrm{St}}$ (Fig. 7) is determined with (eq. 3). Then there must be no horizontal temperature differences, which is true for the end of loading. Here the maximum value $(\mathrm{grad}T_{\mathrm{St}})_{\mathrm{max}}$ is of interest. The maximum temperature gradient is in the thermocline. If the maximum temperature gradient increases, the average height of the thermocline $h_{\mathrm{tc,m}}$, decreases, which has already been described as a target or evaluation criterion (Urbaneck 2009). In Fig. 6 b) the vertical evaluation line is shown, which is located in the centre at $r_{\mathrm{St}}/2$. The application of (eq. 3) is done by evaluating the temperature differences ΔT between the cells, which have a distance of Δy (eq. 4). The maximum value is then searched in the evaluation.

$$\mathrm{grad}T_{\mathrm{St}} = \frac{\partial T_{St}}{\partial h_{St}} \qquad \text{(eq. 3)}$$

$$\mathrm{grad}T_{\mathrm{St}} \cong \frac{\Delta T_{St}}{\Delta y} \qquad \text{(eq. 4)}$$

The average temperature of the hot zone $T_{\mathrm{hZ,m}}$ is the third evaluation criterion related to the hot zone. In *Ansys CFX Post*, the *isovolume* of the hot zone is evaluated. Here the following condition is valid: $T_{\mathrm{St}} > T_{\mathrm{St,90\%}}$.

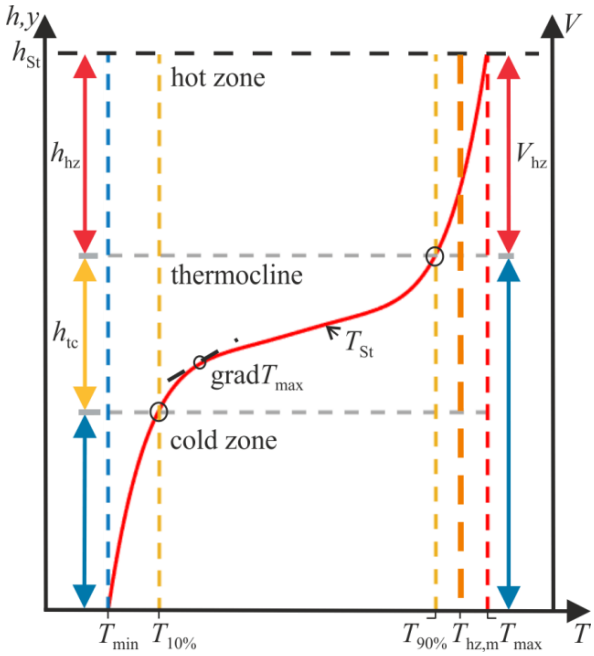

Fig. 7: Schematic representation of the vertical temperature distribution in a displacement storage and important parameters, in accordance with (Urbaneck, 2009)

4. Results

Diffuser model

The calculation of the flow in the connecting pipe and in the diffuser is intended to represent the realistic outflow behaviour into the storage tank. Here, only one sector of the storage space was modelled (Fig. 6). This procedure assumes a uniformly distributed outflow over the entire radius (direction, velocity, mass or mass flow). In reality or in a full three-dimensional simulation, a uniform distribution over the radius probably does not exist. This is shown, for example, by simulative and experimental work by (Findeisen, 2018). Thus, the results presented here involve ideal assumptions.

The flow effects in the diffuser are complex and cause a three-dimensional velocity distribution. To analyse the processes, first a perpendicular or curved section plane is placed in the section (Fig. 6 a)). This is followed by an observation of the velocity in the guide channel (room between two internal elements) perpendicular to the main flow direction.

The velocity profile in the diffuser (vertical section plane in Fig. 6 a)) for the *RD b*, *RD IE 128 50° b* and *RD IE 32 10° b* variants is provided in Fig. 8. The vectors show the main flow direction. This view is in the Z^+ axis in the middle of the section. In the transition area from the connecting pipe into the radial diffuser, the flow accelerates (red area), meets the upper diffuser wall and follows the curved guide channel (Fig. 8). A recirculation area (flow against the main flow direction in the guide channel) is formed in the lower diffuser area. This causes mixing effects at the diffuser outlet, especially at the beginning of the loading process. This is disadvantageous, but cannot be completely ruled out with the measures described here.

This is followed by an examination of the processes in the guide channel. Because the guide channel is curved, *Görtler* vortices are formed in addition to the effects shown above in Fig. 9 (Görtler 1940, Saric 1994). When a certain velocity is exceeded, boundary layer effects occur. Pressure gradients form between the flow close to the wall (outside of the guide channel) and the flow far from the wall in the guide channel. This results in a flow away from the wall (secondary flow) into the inner channel area with lower pressures. This flow behaviour with counter-rotating vortices is shown in Fig. 9 b). The vortices cover large parts of the guide channel and are transported out of the guide channel with the main flow direction. So-called longitudinal vortices are formed. This flow behaviour is confirmed by Fig. 10.

The following tendencies and theories can be read from the diagrams:

- A higher swirl angle β increases the formation of the counter-rotating vortices (Fig. 10 b)).
- A lower number of guiding channels results in a larger recirculation area (Fig. 10 c)).
- Both of the above effects favour the formation of *Görtler* vortices.

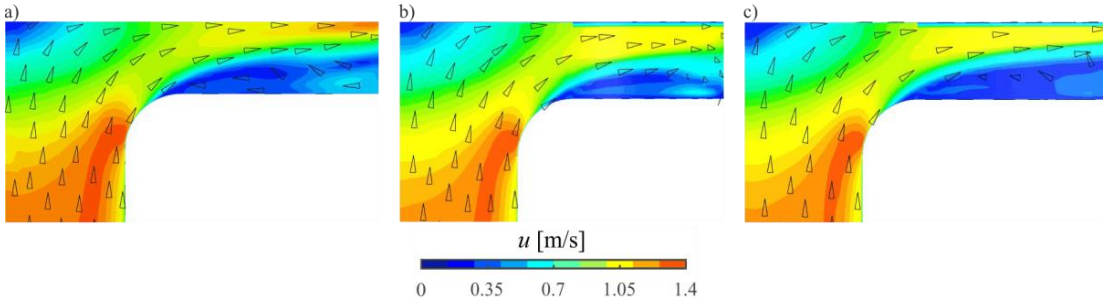

Fig. 8: Velocity with direction vectors in the centre of the section for a) *RD b*, b) *RD IE 128 50° b*, c) *RD IE 32 10° b*

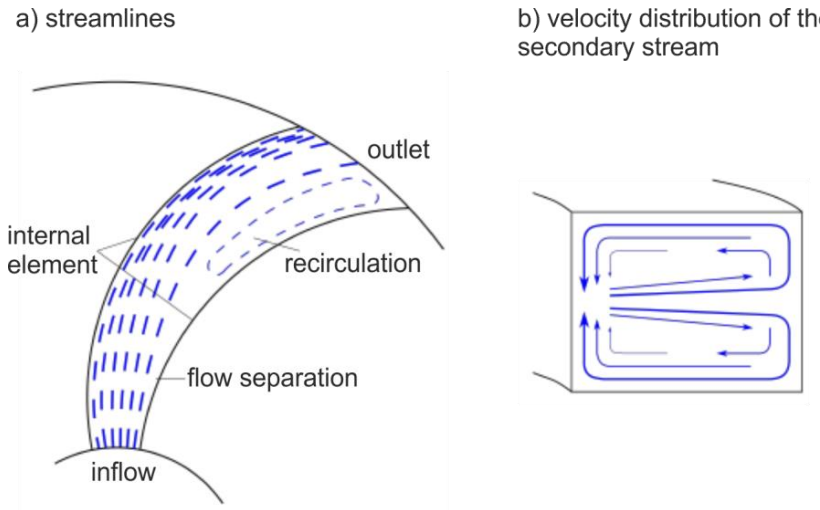

Fig. 9: a) schematic representation of the flow through the curved guiding channel (horizontal section) with the main flow direction and b) velocity arrows of the secondary flow across the flow cross-section (vertical section) in a guiding channel

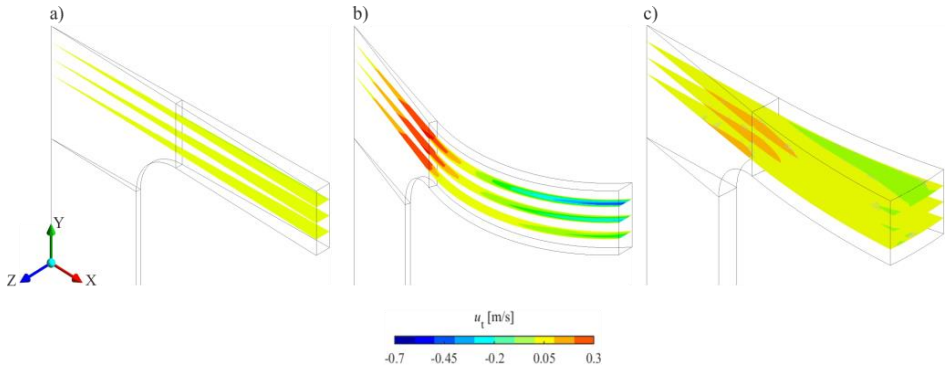

Fig. 10: Tangential velocity component (contour) for a) *RD b*, b) *RD IE 128 50° b*, c) *RD IE 32 10° b*

Fig. 11 a) shows the average velocity amounts and the velocity distributions over the diffuser outlet and the outlet at the guide channel. The *RD IE 128 50° b* variant has the lowest velocity differences. This "nose-shaped" velocity distribution (reversed here) with a velocity maximum near the diffuser wall flowed against by the pipe is often encountered and does not represent a problem in principle with density flows in flat-bottom tanks. The *RD b* variant has larger velocity differences compared to the variant and *RD IE 32 10° b* and *RD IE 128 50° b*. Significantly higher velocities occur in the upper range.

The conventional radial diffuser *RD b* has a horizontally layered distribution of velocities (Fig. 11 b)). The radial diffusers with swirl generation (*RD IE 128 50° b, RD IE 32 10° b*) show clearly different velocities in the

horizontal (Fig. 11 c) and d)), which can be explained by the additional effect of the *Görtler* vortices. A backflow may occur. This cannot be read from the magnitude of the velocity ($u = \sqrt{{u_a}^2 + {u_r}^2 + {u_t}^2}$) in Fig. 11 a)).

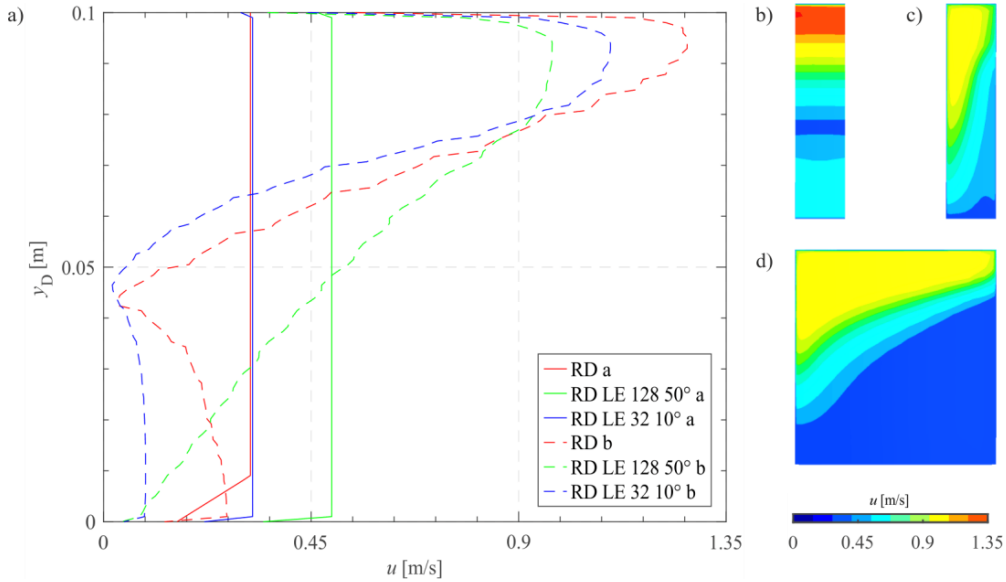

Fig. 11: a) magnitude of velocity and velocities over diffuser height at diffuser outlet and velocity distributions over outlet surfaces for b) RD b, c) RD IE 128 50° b, d) RD IE 32 10° b

Storage model

The effect of the inlet flow at the conventional radial diffuser (variant *RD b*) for different times is shown Fig. 12 a). The flow from the diffuser has the highest velocity. Consequently, a high momentum hits the storage wall. A typical wall jet is formed, which penetrates deep into the storage and causes mixing processes. When the temperature and density differences decrease due to advanced loading (t = 250 s), the penetration depth of the wall jet increases. The *RD IE 32 10° b* variant does not differ significantly from the *RD b* variant. The low swirl angle leads to a marginal weakening of the wall jet. The storage fluid in the upper storage area is moved slightly. For this reason, this variant is not shown.

The flow with swirl for different times and the variant *RD IE 128 50° b* is shown in Fig. 12 b). The inlet flow with swirl differs fundamentally from the previously described flow behavior. The flow enters the storage with a deflection angle and generates a rotation of the storage fluid in the upper storage area. This reduces the momentum impinging on the storage wall. The wall jet or its penetration depth decreases (Fig. 12 b), t = 50 s). With increasing loading time, the rotation of the storage fluid increases (Fig. 12 b), t = 150 s). At the end of loading, the storage fluid of the hot zone is in motion (Fig. 12 b), t = 250 s).

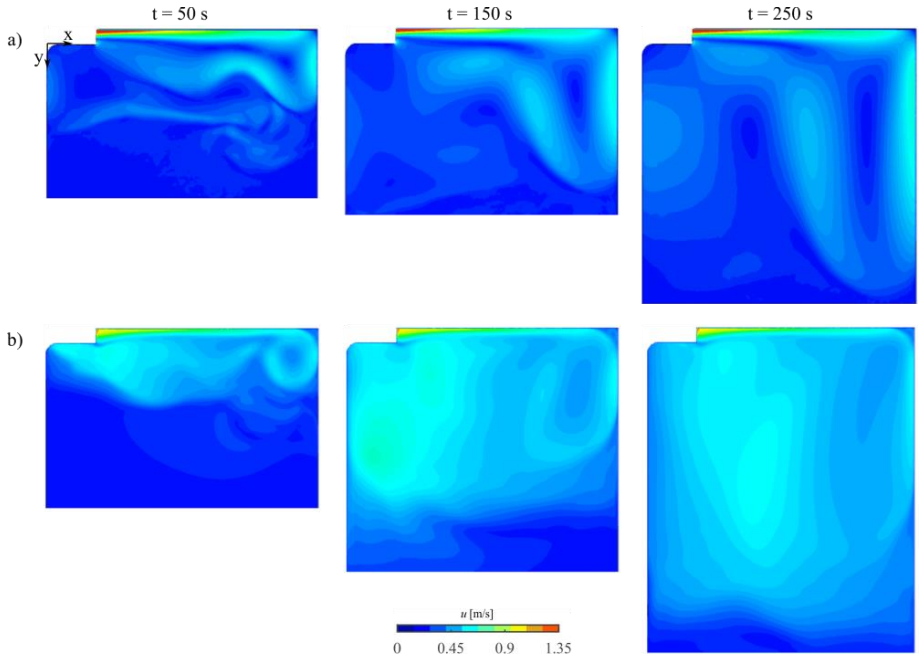

Fig. 12: Velocity fields in storage region for different times and for the variants a) *RD b*, b) *RD IE 128 50° b*

Fig. 13 presents the development of the average height of the thermocline. The *RD a*, *RD IE 128 50°* a and *RD IE 32 10° a* variants consistently deliver better results than the *RD* b, *RD IE 128 50° b* and *RD IE 32 10° b* variants. This can be explained by the uniform distribution of the inlet flow (direction, velocity). This confirms the approach with the reduction of inlet velocities. However, the technical implementation is difficult, as this investigation shows.

The relatively strong increase in variant *RD b* is due to the flow (e.g. effect of the wall jet) or the stratification structure and the evaluation with *isosurfaces*. The lower gradients for the variants *RD IE 128 50° b* and *RD IE 32 10° b* also confirm the reduction of the space in which mixing effects take place.

The above statements on the quality of the thermal stratification are also supported by the key figures in Tab. 2. supplemented by the vertical temperature distributions. Assuming that all variants *b* were modelled more realistically, variant *RD IE 128 50° b* achieves the best stratification quality. The variant provides by far the best results in the evaluation with the height of the thermocline $h_{\mathrm{tc,m}}$ and the maximum temperature gradient $(\mathrm{grad}T_{\mathrm{St}})_{\mathrm{max}}$. The average temperature in the hot zone does not differ so much from the other variant *RD IE 32 10° b* with swirl loading.

Tab. 2: Evaluation of the quality of the thermal stratification with key figures

key figures \ **variant**	***RD a***	***RD IE 128 50° a***	***RD IE 32 10° a***	***RD b***	***RD IE 128 50° b***	***RD IE 32 10° b***
average height of thermocline $h_{\mathrm{tc,m}}$ [m]	0.21	0.31	0.26	0.51	0.36	0.48
max. temperature gradient $(\mathrm{grad}T_{\mathrm{St}})_{\mathrm{max}}$ [K m^{-1}]	281.4	222.0	273.3	175.7	225.3	147.4
average temperature in the hot zone T_{hz} [°C]	123.85	123.35	124.05	121.65	122.95	122.55

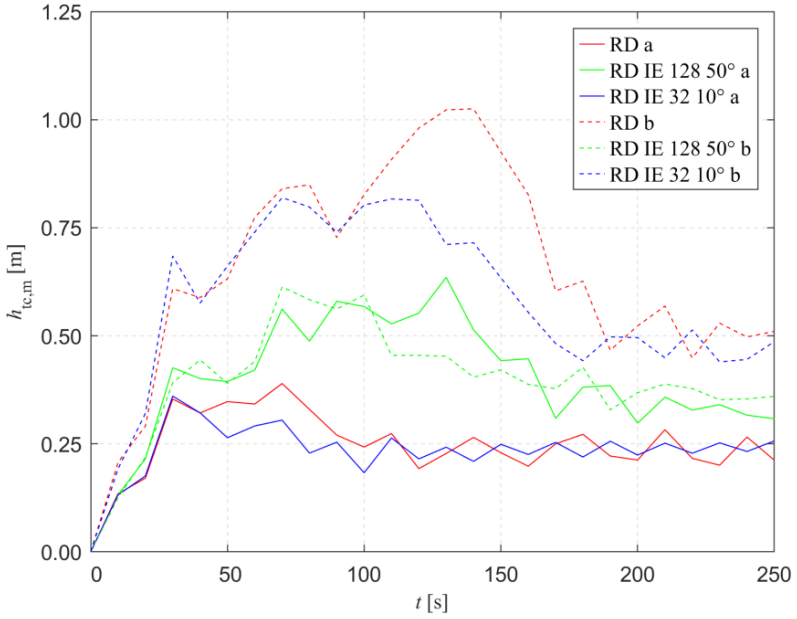

Fig. 13: Development of the average height of the thermocline

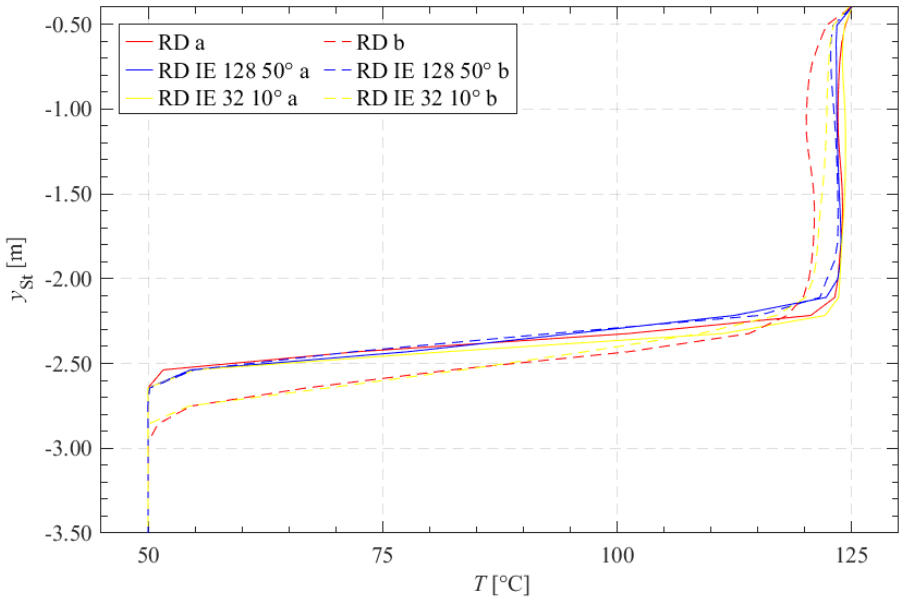

Fig. 14: Vertical temperature curves at $r_{St}/2$ (Fig. 6 b)) for all variants

5. Conclusion and Outlook

More efficient storage solutions are urgently needed to further integrate renewable energy sources and increase system efficiency in heat supply. Hot water storage tanks with a slim design can play a key role (Fig. 1, storage tank type b1)). Here, the internal losses must be minimized or the stratification behaviour improved. An essential prerequisite for this is a sufficiently precise understanding of flow and heat transfer processes during loading. The present work is intended to contribute to closing these knowledge gaps.

Three different diffuser designs (one conventional diffuser and two diffusers with swirl generation) are compared in this work for the improvement of stratification operation. A model for the diffuser with piping and a model for the storage are used in this work. An ideal and a realistic inlet flow with and without swirl generation are compared. The ideal inlet flows show the theoretical potential of perfect velocity decay. Furthermore, new flow effects in slim hot water stores were identified. In the radial diffuser with swirl generation, recirculation flows and so-called *Görtler* vortices are formed due to the wall effects of the curved guide channels. This fundamentally

changes the inlet flow into the storage compared to the conventional radial diffuser. The rotating and specially distributed inlet flow causes the upper storage volume to rotate, the momentum of the wall jet is weakened, and large-scale mixing effects in the upper storage area are reduced. With increasing loading time, the rotation of the storage mass increases. The studies show the advantages of swirl loading over loading with conventional diffusers in slim storage. Future studies aim to improve the understanding of the cause-effect mechanism of swirl loading. This will result in design recommendations of radial diffusers with swirl for different geometries and load cases.

6. Acknowledgement

This article is based on the cooperative project Innovative Loading Systems for Slim Hot Water Storage Tanks (InnoBeS). The Federal Ministry funds the joint project for Economic Affairs and Climate Action through the German Federation of Industrial Research Associations (AiF) as part of the Central Innovation Program for SMEs (ZIM) based on a resolution of the German Bundestag (ZF4746701ST9, ZF4147603ST9). Special thanks go to Dr. Ralf Hartmann of the AiF. The project is carried out in cooperation with the company Harald Liebers Behälterbau GmbH. Many thanks for the constructive cooperation.

7. References

ANSYS, Inc., 2019. ANSYS CFX 2019 R2. Canonsburg (USA).

AG Energiebilanzen e.V.: Anwendungsbilanzen zur Energiebilanz Deutschland, 2020. URL: ag-energiebilanzen.de, accessed on 23.07.2022.

Brämer, C., Urbaneck, T., Lohse, R., 2012. Influence of Geometry and Operation Parameters on Thermal Stratification. EuroHeat&Power, English Edition VWEW Energieverlag, Volume 9, Edition 4, pp. 30-36, ISSN 1613-0200.

Bundesministerium für Umwelt, Naturschutz, nukleare Sicherheit und Verbraucherschutz, 2022. Ziele des Übereinkommens von Paris. URL: www.bmuv.de, accessed on 23.07.2022

Findeisen, F., Urbaneck, T., Platzer, B., 2016. Radiale Diffusoren in Warmwasserspeichern – Funktionale Optimierung mittels CFD; Teil 1 Grundlagen und Modellierung, 2016. HLH Lüftung/Klima Heizung/Sanitär Gebäudetechnik. Volume 76, Edition 10, pp. S. 20-28, ISSN 1436-5103.

Findeisen, F., 2018. Radiale Diffusoren in Warmwasserspeichern – Einfluss der Beladergeometrie auf Strömungsverhalten und Schichtungsqualität. PhD Thesis, TU Chemnitz, ISBN 978-3-9811424-7-1.

Görtler, H., 1940. Über den Einfluss der Wandkrümmung auf die Entstehung der Turbulenz. Zeitschrift für Angewandte Mathematik und Mechanik, Volume 20, Edition 3.

Kroll, U., Mücke, J., Urbaneck, T., Platzer, B., 2020a. Radiale Diffusoren mit Drallerzeugung für schlanke Speicher - Teil 1: Grundlagen und Aufbau des Versuchsstands. HLH Lüftung/Klima Heizung/Sanitär Gebäudetechnik VDI Fachmedien, Volume 71, Edition 5-6, pp. 43-47, ISSN 1436-5103.

Kroll, U., Mücke, J., Urbaneck, T., Platzer, B., 2020b. Radiale Diffusoren mit Drallerzeugung für schlanke Speicher - Teil 2: Vorstellung und Auswertung der experimentellen Ergebnisse. HLH Lüftung/Klima Heizung/Sanitär Gebäudetechnik VDI Fachmedien, Volume 71, Edition 5-6, pp. 56-61, ISSN 1436-5103.

Lohse, R., Urbaneck, T., Brämer, C., Platzer, B., 2012. Effects during loading of hot water storages with a high aspect ratio. EuroHeat&Power, English Edition VWEW Energieverlag, Volume 9, Edition 3, pp. 42-47, ISSN 1613-0200.

Platzer, B., Findeisen, F., Urbaneck, U., Winkler, T., 2017. Verfahren und Vorrichtung zum Be- und/oder Entladen eines thermischen Energiespeichers, 2017. Patent Registration, 2017120716373300DE, Received on: 07.12.2017.

Saric W. S., 1994. Görtler Vortices. Annual Review of Fluid Mechanics, Volume 26:1, pp. 379- 409.

Stahlhut, M., Ackermann, C., Urbaneck, T. , 2022a. Exemplarische Untersuchung verschiedener Kollektoren zur Einbindung in Fernwärmenetze. EuroHeat&Power, VDE Verlag, Volume 51, Edition 01-02, pp. 40-48, ISSN 0949-166X.

Stahlhut, M., Ackermann, C., Urbaneck, T., 2022b. Exemplarische Untersuchung verschiedener Kollektoren zur Einbindung in Fernwärmenetze – Teil 2. EuroHeat&Power. VDE Verlag, Volume 51, Edition 03, pp. 44- 53.

ISSN 0949-166X.

Urbaneck, T., Möller, H., Kressner, T., Platzer, B., 2009. Kaltwasserspeicher mit radialen Diffusoren. Teil 2a: Schichtungsaufbau im Nahfeld - Grundlagen, Physik, Simulation. HLH Lüftung/Klima Heizung/Sanitär Gebäudetechnik, Volume 60, Edition 6, pp. 32-36. ISSN 1436-5103.

Urbaneck, T., Held, A., Platzer, B., 2011. Kaltwasserspeicher mit Rohrdiffusoren – Teil 3b: Einfluss der Betriebs- und Geometrieparameter. HLH Lüftung/Klima Heizung/Sanitär Gebäudetechnik, Volume 62, Edition 4, pp. 31-37. ISSN 1436-5103.

Urbaneck, T., 2012. Kältespeicher: Grundlagen, Technik, Anwendung. Oldenbourg Verlag, ISBN 3486719882.

Urbaneck, T., Oppelt, T., Fischer, J., Sehwöster, E., Bank, E. F., 2019. Große Druckbehälter als thermische Energiespeicher, Teil 2: Umsetzungsbeispiel. EuroHeat&Power, VWEW Energieverlag, Volume 48, Edition 01-02, pp. 32-42. ISSN 0949-166X.

Urbaneck, T., 2020. Water Tank Stores for Medium/Large Applications. Reference Module in Earth Systems and Environmental Sciences, Elsevier, ISBN 9780124095489.

Wagner, W., Kretzschmar, H., 2008. International steam tables: Properties of water and steam based on the industrial formulation IAPWS-IF97. Springer-Verlag Berlin Heidelberg. ISBN 978-3-540-74234-0, DOI https://doi.org/10.1007/978-3-540-74234-0.

Winkler, T., 2017. Radiale Diffusoren mit Drall – Grundlegende Untersuchungen für schlanke Speicher mit Drall. Bachelor Thesis, TU Chemnitz.

8. List of Symbols

Quantity	Symbol	Unit
average height of thermocline	$h_{\mathrm{tc,m}}$	m
entry angle	α	°
height	h	m
mass flow rate	$\dot{m}$	kg s^{-1}
number of internal elements	z	-
pressure	p	Pa
radius	r	m
swirl angle	β	°
temperature	T	°C
temperature gradient	grad$T$	K m^{-1}
time	t	s
velocity	u	m s^{-1}
vertical coordinate	y	m
volume	V	m³

Shortcut	Meaning
a	axial
c	critical
CFD	Computational Fluid Dynamics
Char	charging
CP	connecting pipe
D	Diffuser
hz	hot Zone
IAPWS-IF97	The International Association for the Properties of Water and Steam - Industrial Formulation 1997
IE	internal element
max	maximal
min	minimal
r	radial
rel	relative
RD	radial diffuser
RD IE	radial diffuser with internal elements
S	Set
St	Storage
Su	Supply
t	tangential
32 / 128	number of internal elements
10° / 50°	angle of swirl